Micromixing in a Single-Feed Semi-Batch Precipitation Process

R. Phillips and S. Rohani
Dept. of Chemical Engineering, Thorvaldson Bldg., University of Saskatchewan, Saskatoon, S7N 5C9, Canada

J. Baldyga
Dept. of Chemical and Process Engineering, Warsaw University of Technology, PL-00-645 Warsaw, Poland

A mixing-precipitation model (based on engulfment, the E-model by Baldyga and Rohani, 1987) is applied to a single-feed semi-batch precipitation process to describe the mixing effects on the final particle-size distribution (PSD) and particle morphology. The model describes mixing on two scales: the microscale (at which the flow directly affects nucleation and growth phenomena in the mixed-precipitation (MP) zone) and a macroscale (which controls the environment for the MP-zone). Application of the model is limited to $1 \ll Sc < 4{,}000$ and slow feed addition rates. When the model was applied to experimental results of $BaSO_4$ precipitation, satisfactory agreement between predicted and observed results was obtained. Experiments were carried out in a single-feed 18-L Rushton reactor, whereby the effects of various operating conditions such as feed rate, intensity of mixing, mean initial reactant concentration and reactant volume ratio on barium sulfate precipitation process were investigated.

Introduction

Precipitation processes find important applications in the production of pigments, photographic materials, and pharmaceutical products. The majority of chemical engineering design and modeling approaches to crystallizers assume that the system is perfectly mixed. However, depending on the mode of operation and operating conditions, mixing may become the rate-controlling step for fast precipitation systems. The experimental studies on $BaSO_4$ precipitation show significant mixing effects: Pohorecki and Baldyga (1983) observed a decrease in the mean particle size with an increase of impeller speed for batch precipitation. In the case of the continuous precipitation process in stirred-tank reactors, an increase in the particle size was observed (Fitchet and Tarbell, 1990), whereas in the case of semibatch precipitation, a minimum on the curve of particle size vs. impeller speed was obtained (Tosun, 1988). It is impossible to predict these trends intuitively; however, it is clear that mixing affects generation of supersaturation and its redistribution in a system. It is therefore necessary to incorporate a suitable mixing model to reactive precipitation processes to predict the final product characteristics (yield, particle morphology, mean size, PSD, and so on). Chemical reaction, nucleation, and crystal growth are molecular level processes, therefore, only mixing on molecular scale can directly influence their course. For the same reason, any linking of precipitation kinetics with mixing models should be done locally on the level of a phenomenological point. The macroscopic flow pattern (macromixing), as well as turbulent diffusion and inertial-convective mixing (mesomixing), determine the environment for micromixing and have indirect influence on precipitation. The influence of mixing on the crystal-size distribution has been studied either by modeling the supersaturation distribution and solid-phase distribution with the use of environmental and mechanistic micromixing models (Pohorecki and Baldyga, 1983; Garside and Tavare, 1985; Baldyga et al., 1995; Marcant and David, 1991; Aslund and Rasmuson, 1992; Podgórska, 1993; David and Marcant, 1994; Chen et al., 1996) or by using closure schemes combined with CFD simulations (Pipino et al., 1994; Baldyga and Orciuch, 1997). Modeling yielded several interesting as well as contradictory (on the first view) results. Using micromixing models, Pohorecki and Baldyga (1983) pre-

Correspondence concerning this article should be addressed to S. Rohani.

dicted the opposite mixing effects on the particle size in batch and continuous stirred-tank reactors. Predictions by the engulfment micromixing model have shown that in the case of a single-feed semi-batch precipitation an increase of impeller speed can decrease or increase the size of the precipitated particles. A combination of the viscous-convective mixing (engulfment) with the macroscopic flow was shown to give better agreement with experimental data (Podgórska, 1993). The double-feed semi-batch precipitation process of calcium oxalate was studied by David and Marcant (1994). Using a semi-quantitative approach, they were able to predict the trends of the effect of volume ratio, stirrer speed, and feed pipe location on the mean crystal size. The multiple-time-scale model describing the interactions between large-scale convection, inertial-convective mesomixing, and viscous-convective micromixing was applied recently to the process of a double-feed semi-batch precipitation of barium sulfate (Baldyga et al., 1995). Changes observed in particle morphology were interpreted using precipitation diagrams. Chen et al. (1996) have considered the interactions between macromixing and micromixing, which can explain the appearance of a minimum on the mean particle size vs. impeller speed, as observed experimentally by Tosun (1988). Similar results like in the case of simple mechanistic models are obtained when using the closure schemes often combined with the CFD models (Pipino et al., 1994; Baldyga and Orciuch, 1997) or using CFD with neglected fluctuation terms (Wei and Garside, 1997). Depending on the process conditions, results of computations show, also in this case, contradictory trends, which agree in many cases with experimental data. The ''closure-CFD'' models are presently evolving, and it is expected that in a few years they will be in use. Simple mechanistic models based on physics of mixing and verified experimentally (using complex reactions, as well as precipitation) are presently preferable for the simulation of precipitation sensitivity to process parameters. The multiple-time-scale mixing model including process of viscous-convective micromixing (engulfment) is one possible proposition.

Mixing-Precipitation Model

Mixing model

The general mixing-precipitation model should consider all mixing phenomena which directly or indirectly affect the chemical reaction, nucleation, and growth of particles. They are briefly presented in what follows.

Macromixing is the process of mixing on the scale of the vessel. It conveys fluids through environments where the turbulent properties and composition vary. The characteristic macromixing time in a stirred tank can be expressed by the mean circulation time

$$t_c = \frac{V}{q_c} \tag{1}$$

Turbulent diffusion characterizes inhomogeneity of the plume of fresh feed; for slow addition (assuming a point source in a uniform flow). Its characteristic time given by Baldyga and Bourne (1992) estimates the time period after which the probability of interactions of fluid elements emerging from the point source becomes negligible

$$\tau_D = \frac{q_B}{\bar{u} D_t} \tag{2}$$

where $\bar{u}$ represents the local average velocity (m/s).

The inertial-convective mixing (mesomixing) describes a coarse scale segregation of reactants with the scales of inhomogeneity larger than the Kolmogorov microscale and smaller than the integral length scales of turbulence (the inertial-convective subrange). The time constant pertaining to this aspect of mixing (Corrsin, 1964), is given by

$$t_{ms} \cong \frac{3}{2} k_{oc}^{-2/3} \epsilon^{-1/3} = \frac{3}{2} \left(\frac{5}{\pi} \right)^{2/3} \Lambda_c^{2/3} \epsilon^{-1/3} \tag{3}$$

Micromixing in the case of liquids ($Sc \gg 1$) represents mixing in the viscous-convective and the viscous-diffusive subranges of concentration spectrum. Mixing in both subranges can be represented by the engulfment-deformation-diffusion (EDD) model (Baldyga and Bourne, 1984). For Schmidt numbers ($Sc \ll 4{,}000$) which are not too high, the viscous-diffusive effects are negligible and the intensity of micromixing is represented by the engulfment intensity parameter E (1/s) (Baldyga and Rohani, 1987).

$$E = 0.058 \cdot \left(\frac{\epsilon}{\nu} \right)^{0.5} \tag{4}$$

where the E parameter is proportional to the Kolmogorov rate of strain with the proportionality constant reflecting the highest vorticity of turbulence. The time constant for engulfment(s) $t_E \cong 1/E$.

Predictions of the full multiple-time-scale model show good agreement with experimental data for complex reactions. For very slow feeding, the model can be reduced to macromixing and engulfment, still yielding a good agreement with experimental data (Bourne and Yu, 1994).

Precipitation

Reactive precipitation includes chemical reaction leading to supersaturation, nucleation, and growth of crystals. The chemical reaction between barium chloride and sodium sulfate is very fast. The reaction time constant is 8 orders of magnitude smaller than micromixing due to engulfment. The nucleation time estimated by the induction time t_{ind} (s), (Dirksen and Ring, 1991) is given by

$$t_{\text{ind}} = \frac{6 d_m^2 n^*}{D_i \ln S} \tag{5}$$

The characteristic time for the crystal growth can be expressed in terms of the product concentration decrease resulting from the crystal growth (Baldyga et al., 1995)

$$t_G = \left(\frac{\rho \cdot G}{2M} \cdot a \right)^{-1} \cdot \overline{C_c} \tag{6}$$

At any given operating condition, the nucleation and growth time constants for the barium sulfate precipitation were found to be at least eight and four orders of magnitude smaller, respectively, than the engulfment time constant.

In the present work the time of semi-batch operation is much longer than the circulation time; therefore, one can assume uniform composition of the bulk contacting the micromixing zone. Equation 2 shows that at small values of q_B, the effects of turbulent diffusion are negligible. Similarly, for slow feeding from a nozzle, the fresh feed relaxes to the environment velocity and the continuity relation ($q_B = \pi \Lambda_c^2 \bar{u}$) yields $\Lambda_c \approx [q_B/(\pi \bar{u})]^{1/2}$ for the concentration scale. Hence, one can make the initial value of t_{ms} ($t_{ms} \propto \Lambda_c^{2/3}/\epsilon^{1/3}$) which is smaller than $1/E$. This does not have any physical meaning; thus, only the viscous-convective mechanism of mixing should be employed in the model. The maximum in supersaturation, as well as maximum in nucleation rate, are reached after $t \cong \ln 2/E$. The order of the homogeneous nucleation rate is so high that small dilution of supersaturation practically stops nucleation. Hence, interaction between mixing and nucleation during a short period of time $\Delta t \approx 1/E$ determines number of crystals and PSD.

One can conclude that the model of a semi-batch precipitation process at low feed addition rate should include mixing on macroscale (history of environments) and the viscous-convective micromixing (exchange with the environment).

Application to a Single-Feed Semi-Batch Process

The single-feed precipitation process is shown in Figure 1. Macromixing is simulated in the model by using a loop plug flow with the circulation capacity recalculated from a pumping capacity of the impeller

$$q_c = C_1 \cdot Q_p \qquad C_1\text{: bulk entrainment coefficient} \qquad (7)$$

$$Q_p = C_2 \cdot (Nd^3) \qquad C_2\text{: impeller discharge coefficient} \qquad (8)$$

The coefficients C_1 and C_2 for the pitched-blade turbine were taken as 2 and 0.75 (Oldshue, 1983; Fort, 1986). The spatial inhomogeneity in the system is reflected by updating the corresponding engulfment parameter values that depend on the age (t) of the MP-zone on the Lagrangian trajectory (see Figure 1). Several authors (Okamoto et al., 1981; David and Villermaux, 1987; Wu and Patterson, 1989; Geisler, 1991; Bourne and Yu, 1994) have formulated maps to describe the velocity and energy dissipation rate distributions within a mixed reactor. In this work, the energy dissipation rates are described by employing a method formulated by Okamoto et al. (1981), which divides the reactor content into a bulk volume (V_b) and an impeller volume (V_i) that have considerably different local energy dissipation rates (m^2s^3) (ϵ_b and ϵ_i, respectively). Applying Okamoto et al. (1981) correlations for the tank geometry used for the experimental work (as will be seen in Figure 3), $V_i/V = 0.051$; $\phi_i = (\epsilon_i/\bar{\epsilon}) = 15.0$, and $V_b/V = 0.949$; $\phi_b = (\epsilon_b/\bar{\epsilon}) = 0.25$. Zhou and Kresta (1996a,b) have shown that for a pitched-blade turbine with $d/D = 0.5$, 72% of the energy is dissipated in the zone of $z \cong 0.14$ and 54.85% in the zone of $z \cong 0.07$. The correlation of Okamoto et al. (1981) predicts 62% in the zone of $z \cong 0.105$.

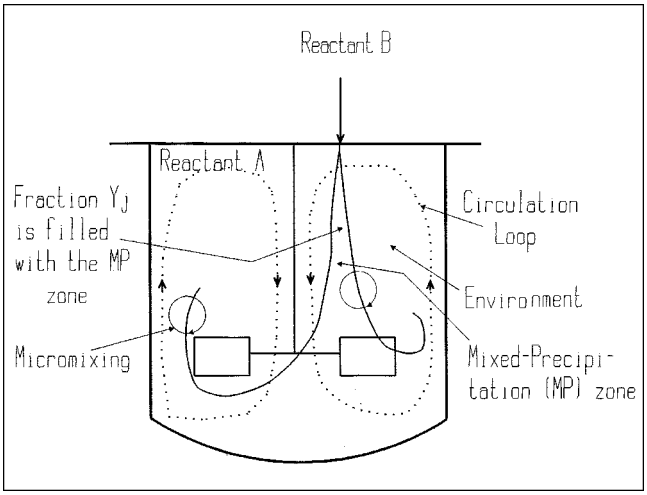

Figure 1. Mixing-precipitation model.

The mean energy dissipation rate can be calculated using the power number N_P, tank and impeller geometry

$$\bar{\epsilon} = \frac{4 N_p N^3 d^5}{\pi D^2 H} \qquad (9)$$

For a pitched-blade turbine and the prevailing experimental system, a value of $N_P = 1.5$ (Uhl and Gray, 1966) can be used with 15% reduction for a dished-bottom tank (Post, 1983). The velocity distribution of the MP-zone within the tank was simulated employing the idea of the experimental flow model (Bourne and Yu, 1994), which yielded the local values of the rate of energy dissipation for the fluid elements wandering in the system. The feed stream is discretized into parts with volume $q_B t_c$. This reflects the fact that the composition of the environment changes (and is updated) with a frequency $1/t_c$. The fresh feed is introduced to the circulation loop at constant flow rate q_B, the initial volume fraction of the B-rich solution in the loop cross section being $Y_j(0;t) = q_B/(q_B + q_c)$. The feed entering the system at time t grows during its residence time in the system t', as a result of engulfing the environment

$$\frac{dV_j(t';t)}{dt'} = E \cdot \left[1 - Y_j(t';t)\right] \cdot V_j(t';t); \qquad V_j(0;t) = q_B \qquad (10)$$

This changes the local (in the loop) value of the volume fraction of the MP zone

$$\frac{dY_j(t';t)}{dt'} = E \cdot \left[1 - Y_j(t';t)\right] \cdot Y_j(t';t); \qquad Y_j(0;t) = q_B/(q_B + q_c) \qquad (11)$$

The concentration profiles of both precipitating ions in the MP-zone can be calculated using the micromixing equations

$$\frac{dC_{ij}(t';t)}{dt'} = E\cdot\left[1-Y_j(t';t)\right]\cdot\left[\langle C_i(t)\rangle - C_{ij}(t';t)\right] - \frac{\rho\cdot G(t';t)}{2M}\cdot a(t';t) \quad (12)$$

with the initial conditions $C_{Aj}(0;t)=0$ and $C_{Bj}(0;t)=C_{B0}$.

The particle-size distribution varies along the plume of the MP-zone. Assuming McCabes' ΔL law and neglecting the breakage and aggregation processes, the macroscopic population balance takes the form

$$\frac{\partial\Psi_j(L,t',t)}{\partial t'} + G\frac{\partial\Psi_j(L,t';t)}{\partial L} = E\cdot(1-Y_j)\left[\langle\Psi(L;t)\rangle - \Psi_j(L,t';t)\right] \quad (13)$$

where Ψ_j, $\langle\Psi\rangle$ refer to the population density ($1/\mathrm{dm}^4$) of the PSD in the MP-zone and environment, respectively. The initial and boundary conditions for Eq. 13 are $\Psi_j(L,0;t)=0$ and $\Psi_j(0,t';t)=R_N(t';t)/G(t';t)$, respectively, where R_N and G are nucleation ($1/(\mathrm{dm}^3\cdot\mathrm{s})$) and growth (dm/s) rates.

Kinetic Parameters

The supersaturation (Δc) ($\mathrm{mol}^2/\mathrm{dm}^6$) for reactive precipitation can be calculated from

$$\Delta c = \sqrt{C_A C_B} - \sqrt{K_s} \quad (14)$$

where K_s is the solubility product of the precipitating product ($\mathrm{mol}^2/\mathrm{dm}^6$). For barium sulfate, the value $pK_s = 9.96$ at room temperature (Templeton, 1960). Nucleation is usually described empirically (Eq. 15) as a function of supersaturation

$$R_N = k_n(\Delta c)^n \quad (15)$$

For barium sulfate precipitation (Baldyga et al., 1995)

$$R_N = 600\times10^{12}(\Delta c)^{1.775} \qquad (\text{for } \Delta c < 0.01 \text{ mol}/\mathrm{dm}^3) \quad (16)$$

$$R_N = 2.53\times10^{39}(\Delta c)^{15.0} \qquad (\text{for } \Delta c > 0.01 \text{ mol}/\mathrm{dm}^3) \quad (17)$$

The growth rate (G) can be derived using the two step model, namely, the turbulent mass transfer from the bulk to a single particle surface, and chemical reaction (Karpinski, 1985)

$$G = k_R\left[\sqrt{[\mathrm{Ba}^{2+}]_i[\mathrm{SO}_4^{2-}]_i} - \sqrt{K_s}\right]^r = k_{DA}\left([\mathrm{Ba}^{2+}] - [\mathrm{Ba}^{2+}]_i\right) = k_{DB}\left([\mathrm{SO}_4^{2-}] - [\mathrm{SO}_4^{2-}]_i\right) \quad (18)$$

where r is the order of the reaction and $k_{DA}=k_{DB}=k_D$ are coefficients related to the particle-mass-transfer coefficient (k_d) by

$$k_D = k_d\cdot M/\rho \quad (19)$$

The measured value of constant k_D lies between 1.0×10^{-4} and 1.0×10^{-3} $(\mathrm{dm}\cdot\mathrm{s}^{-1})(\mathrm{dm}^3\cdot\mathrm{mol}^{-1})$ and assumes no dependence of mass-transfer coefficient on the size of crystals (Nagata and Nishikawa, 1972). An average value of 4.0×10^{-4} was taken for present calculations. Equations 18 and 19 lead to a nonlinear equation for the calculation of growth rate (Fitchett and Tarbell, 1990)

$$\Delta c = \frac{3k_\upsilon\rho G}{k_a k_d} + \left(\frac{3k_\upsilon\rho G}{k_a k_R}\right)^{1/r} \quad (20)$$

where $r=4$. The value of rate constant for surface reaction was estimated as $k_R = 6.3\times10^{11}$ $(\mu\mathrm{m}\cdot\mathrm{s}^{-1})(\mathrm{mol}^{-4}\cdot\mathrm{dm}^{12})$ (Nielsen, 1958). The area and volume shape factors (k_a and k_υ, respectively) relating to the particle morphology have been determined by analyzing the scanning electron microscope (SEM) photographs of the barium sulfate particles (see Figures 2a and 2b) at 8.17 and 1.362, respectively (Podgórska,

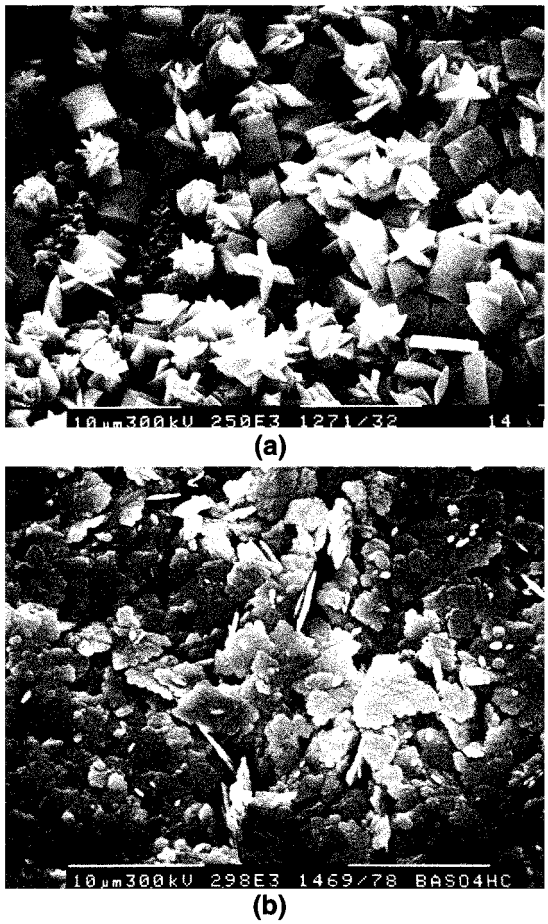

Figure 2. SEM photograph of the precipitate for feed pipe "location I" (below the liquid surface).

(a) At low concentration, $\overline{C}_{B0} = 0.0045$ M; (b) at high concentration, $\overline{C}_{B0} = 0.02$ M.

1993; Baldyga and Orciuch, 1997). The mean specific surface area of the particles per unit volume of the suspension (a) is related to the population density function Ψ_j ($1/\text{dm}^4$) by

$$a = \int_0^\infty k_a \cdot \Psi_j(L) \cdot L^2 \cdot dL \tag{21}$$

The mass weighted mean size (L_{43}) (μm) is given by the ratio of the fourth moment to the third moment of the particle population density

$$L_{43} = \frac{\int_0^\infty \Psi_j(L) \cdot L^4 \cdot dL}{\int_0^\infty \Psi_j(L) \cdot L^3 \cdot dL} \tag{22}$$

The sphericity of a particle and its volume shape factor are related by

$$\phi_v = \left(\frac{\pi}{6k_v}\right)^{1/3} \tag{23}$$

The mean particle size measured during laboratory experiments by the Coulter-Counter (which assumes spherical particles) is compared to d_{43} (μm), which is a measure of the mass weighted mean size having unit sphericity (Eq. 24)

$$d_{43} = L_{43}/\phi_v \tag{24}$$

Another important parameter characterizing the particle-size distribution is the coefficient of variation (C.V.).

$$\text{C.V.} = \frac{\text{standard deviation}}{\text{mean size}} \times 100\% \tag{25}$$

Model Simulation

The equations describing the model for a single-feed semi-batch precipitation process are material balance, the population balance equation, nucleation and growth kinetics using the operating conditions and the flow map. The moment transformation changes the partial differential equation (population balance) into ordinary differential equations as shown below

$$\frac{dm_j}{dt} = jGm_{j-1} + 0^j \cdot R_N + E \cdot (1 - Y_j)(\langle m_j \rangle - m_j)$$

$$j = 0, 1, 2, \ldots \tag{26}$$

The calculation of the mean size and C.V. can be simplified in terms of moments (Randolph and Larson; 1988)

$$d_{43} = \frac{m_4}{m_3 \cdot \phi_v} \quad \text{and} \quad \text{C.V.} = \left(\frac{m_3 m_5}{m_4^2} - 1\right)^{0.5} \tag{27}$$

The set of moment equations can be closed after the fifth moment. The set of simultaneous ordinary differential equations includes seventeen equations, namely, 0th to 5th moments of the MP-zone and the environment; concentrations of A and B in the MP-zone and the environment, and the volume fraction. These equations were solved using IMSL (International Mathematical and Scientific Library) Inc., MATH/LIBRARY v2.0. The equation for growth rate was solved using Newton-Raphson's convergence scheme. The numerical scheme employed was verified using material balance at the end of the simulation with the tolerance being 0.01%.

Experimental Studies

Experiments were carried out in an 18-L Rushton-type tank with a dished bottom (see Figure 3). The impeller and tank diameters were $d = 0.096$ m and 0.290 m, respectively. A pitched blade type impeller was used (having pitch angle of 45°). Figure 4 shows the experimental setup for the precipitation system. Feed (sodium sulfate) was added to barium chloride solution (initial volume, $V_{A0} = 18.0$ dm^3) using tubes of 0.15 cm ID to avoid backmixing. Experiments were conducted for two feed locations—I (near surface) and II (near the impeller), as shown in Figure 3.

Position I: $r_x = 2.5$ cm $\quad z = 28.3$ cm

Position II: $r_x = 2.5$ cm $\quad z = 6.5$ cm

The flow rates from the Masterflex pump No. 7520-25 (Cole Parmer, Barrington, IL) were computer controlled using the Optomux board (OPTO22 Automation, Temecula, CA). To ensure a constant flow rate, the head at the burette end was kept constant. The activity of the ions, and, thus, the progress of reaction was monitored over the entire batch time using

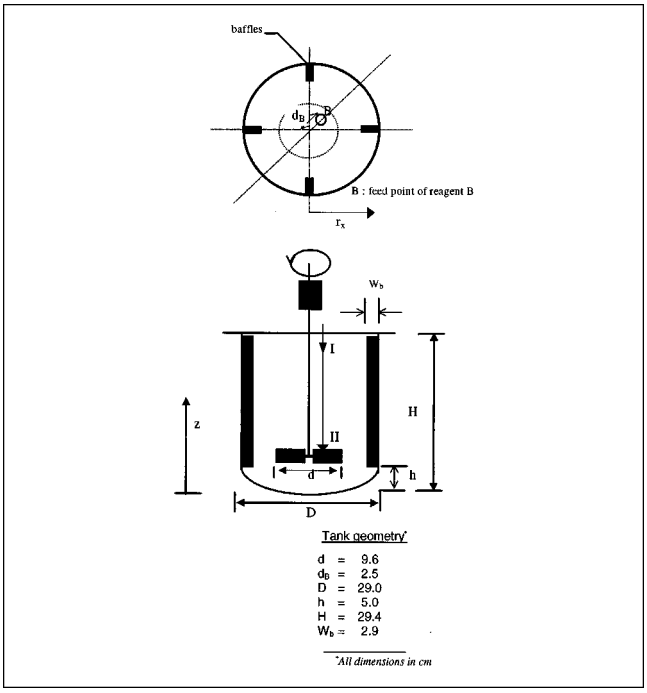

Figure 3. Details of the Rushton tank used.

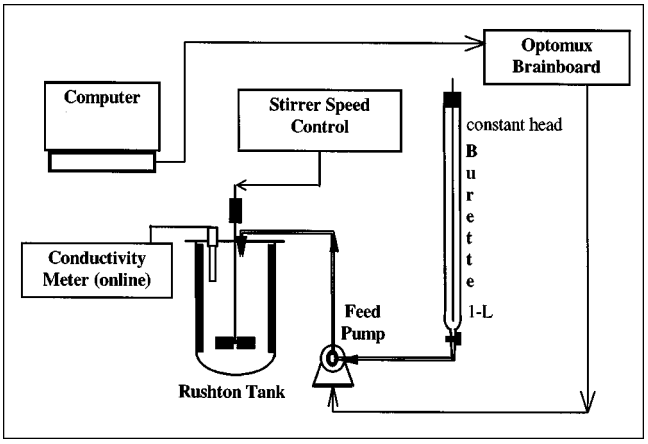

Figure 4. Experimental setup for the micromixing study.

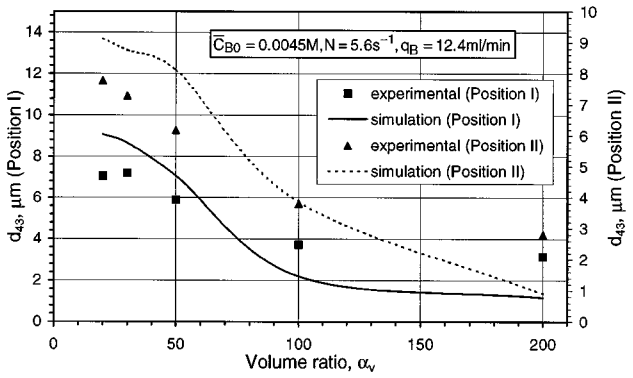

Figure 5. Effect of volume ratio on mean particle size.

the Oakton WD-35607-00 (LABCOR, Que., Canada) basic conductivity meter.

Experiments were conducted to study the effect of operating parameters such as volume ratio (α_v) (V_{A0}/V_{B0}), stirrer speed (N) (L/s), mean initial concentration of the reactants, total feed addition time (t_f) (s), and stoichiometric ratio (η) on the mean particle size and C.V. for the two feed pipe locations. Definitions of volume ratio and stoichiometric ratio are given by

$$\alpha_v = V_{A0}/V_{B0}; \qquad \eta = \frac{\overline{C_{A0}}}{\overline{C_{B0}}} \tag{28}$$

where V_{A0}, V_{B0} are the initial volumes of reactants A and B, respectively. The volume ratio, mean initial concentrations ($\overline{C_{A0}}$ and $\overline{C_{B0}}$), and the actual initial concentrations of A and B (C_{A0} and C_{B0}) are related

$$C_{A0} = \overline{C_{A0}}(1 + 1/\alpha_v); \qquad C_{B0} = \overline{C_{B0}}(1 + \alpha_v) \tag{29}$$

$$C_{i0}V_{i0} = \overline{C_{i0}}(V_{A0} + V_{B0}); \qquad i = A, B \tag{30}$$

The total feed addition time was kept long enough to ensure pure micromixing effects. Table 1 summarizes the operating conditions. Samples were collected at the end of the experiments without delay to eliminate settling effects. Samples from at least three vertical locations in the tank were representative of the experiments. These samples were then filtered and washed with distilled water, and dispersed in Isoton II for PSD analysis using the Coulter-Counter Model TA II (Coulter Electronics, Hialeah, FL). The mass weighted mean size (d_{43}) and the corresponding coefficient of variation (C.V.) were then calculated from the PSD measurements.

Results and Discussion

Effect on particle-size distribution

The effects of various operating conditions on the mean particle size are based on the relative competition between *micromixing* of fluids and *nucleation* and *growth* of the precipitate particles.

Effect of Reactants' Volume Ratio. Figure 5 shows the effect of volume ratio on the mean particle size. The decrease in the mean particle size with increasing volume ratio is due to the fact that, locally, more quantity of B is added at the same flow rate. This results in an increase in local supersaturation, leading to higher nucleation rates, and, therefore, smaller particles. Figure 5 illustrates a comparison of the predicted trends with experimental results. An increase in the volume ratio decreases the size of the particles as predicted, for feeding below the liquid surface as well as feeding near the impeller.

Effect of Mean Initial Concentration. The mean size is very sensitive to the mean initial concentration. The model predicts a very strong decrease of the mean size with increase in the mean initial reactant concentration (Figure 6). It also suggests the appearance of a maximum on the curve, which is testified by experimental results. At low concentrations, the increase in the initial concentration of the reactants favors the growth rate more than the nucleation rate. This is evident from the lower exponential power of the heterogeneous nucleation rate ($n = 1.775$) in comparison to that of the growth rate ($r = 4.0$). However, for larger initial concentrations (and,

Table 1. Experimental Operating Conditions

Parameter	Range				
Feed pipe location	Surface				Impeller
Volume ratio	20	30	50	100	200
Stirrer speed (s^{-1})	1.6	2.6	3.5	5.6	7.5
Mean initial conc. ($mol \cdot dm^{-3}$)	0.0020	0.0045	0.0070	0.0100	0.0200
Total feed addition time (min)	18	21	40	55	75
Stoichiometric ratio	1		2		3

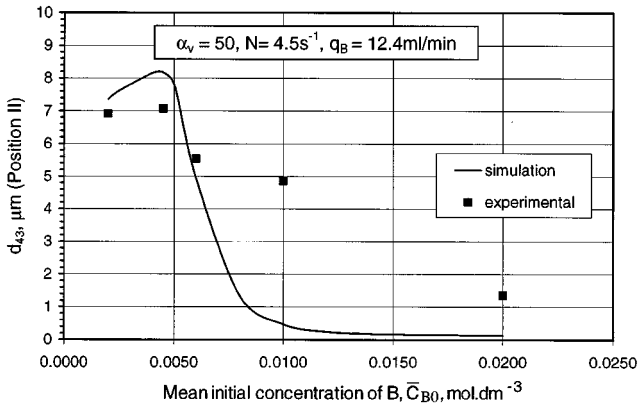

Figure 6. Effect of mean initial concentration on mean particle size for feeding below the liquid surface.

thus, larger supersaturation), the order of nucleation changes from 1.775 (heterogeneous) to 15.0 (homogeneous), thereby producing smaller particles. The experimental mean particle size, however, does not show as large a decrease as predicted by the model.

Increased discrepancies between the model predictions and the experimental data were most probably due to the agglomeration observed in Figure 2b, which had been neglected in the model. The concentration $\bar{C}_{B0} \approx 0.005$ M and the volume ratio $\alpha \approx 100$ form a limit for employing $BaSO_4$ as a test reaction for a single-feed semi-batch precipitation. In the system with no backmixing and for $\alpha = 1$, Baldyga and Orciuch (1997) did not observe agglomeration up to $\bar{C}_{B0} = 0.02$ M. Note, however, that in the semi-batch experiment with $\bar{C}_{B0} =$ 0.02 M and $\alpha = 100$, the feed concentration equals $C_{B0} = 2.02$ M and the existing particles in the suspension can contact a zone of high supersaturation. This promotes agglomeration as observed in Figure 2b.

Effect of Stirrer Speed. There are major contradictions in the literature as to the effect of stirrer speed on the mean size. It has been shown experimentally by model simulations, and by qualitative arguments, that an increase in stirring intensity can increase, decrease, produce a minimum, or not affect the mean crystal size at all. In our case, an increase in the mean particle size with increasing stirrer speed was observed, resulting from faster redistribution of supersaturation at high stirrer speed. Figures 7a and 7b compare model simulations with experimental results for feeding below the liquid surface and near the impeller, respectively. The experimental trends agree with simulation results. Small deviations in the regions of low turbulence intensity may be related to nuclei agglomeration, as explained by Kuboi et al. (1986).

At higher concentrations, a minimum as well as an increase in the particle size were predicted by the model; these effects could not be, however, observed in experiments due to agglomeration effects.

Effect of Feed Addition Time. The effect of feed addition time for feeding below the liquid surface and near the impeller ($N = 1.6$ rps) is shown in Figure 8. Both simulation and experimental results testify to an increase of the mean particle size with an increase in the feed addition time. Increasing the feed addition time is related to a decrease of the feed rate and the volume fraction Y_j (Eq. 11) with a small increase of mixing rate (Eqs. 12 and 13). The increase is more significant when feeding near the impeller (as mixing as faster) there due to higher rate of energy dissipation and higher mixing parameter E.

Effect of Stoichiometric Ratio. A comparison of simulation and experimental results is depicted in Figure 9 for the effect of stoichiometric ratio on the mean particle size. As expected, when reactant A is present in excess of reactant B, the mean size of the particles decreases significantly as supersaturation increases, leading to higher nucleation rates with insufficient amount of B to increase the growth significantly. Experimental deviations could be attributed to the fact that concentrations, instead of the activities of the reactants, have been used in the model. The kinetics were developed experimentally by Nielsen (1958) for a unity stoichiometric ratio, and, therefore, at nonstoichiometric ratios (and, thus,

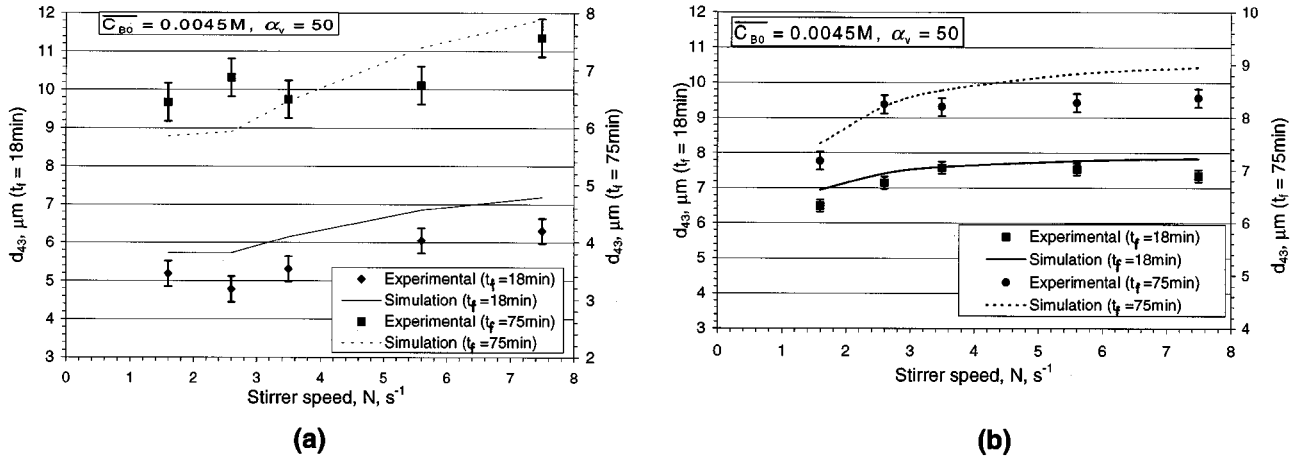

Figure 7. Effect of stirrer speed on mean particle size for feeding.

(a) Below the liquid surface; (b) near the impeller.

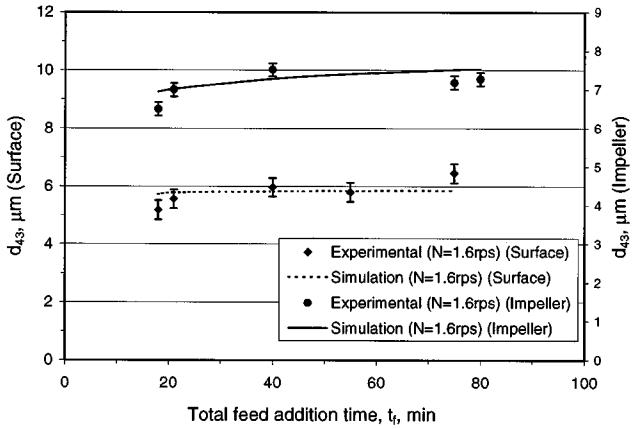

Figure 8. Effect of feed addition time on mean particle size.

higher concentrations of one of the reactants), deviations from the predictions can be expected.

Another important parameter describing the final product characteristics is the coefficient of variation (C.V.). For the first feed pipe location, it was observed that only the stirrer speed exhibits a significant effect on C.V. An increase in the stirrer speed always decreases the C.V. (see Figures 10a and 10b). Also, feeding near the impeller reduces the coefficient of variation (Figure 10c), as feeding is now directly into the region of high turbulence intensity. It can also be observed that almost the same mean size of the particles can be obtained by altering the combinations of operating conditions (in this case, feeding near the impeller at low stirrer speed instead of feeding below the liquid surface at high stirrer speed). In the impeller region, the nucleation and growth of crystals become completely separate and the crystals grow uniformly in the well-mixed region. For position II of the feed pipe, an increase in volume ratio increases the coefficient of variation (see Figure 11). No other operating parameter had a significant effect on the C.V. for the second location of the feed pipe. Generally, a decrease in C.V. can be related to shorter periods of fast nucleation (see Figure 12), which can be achieved by increasing stirrer speed and changing the feed position.

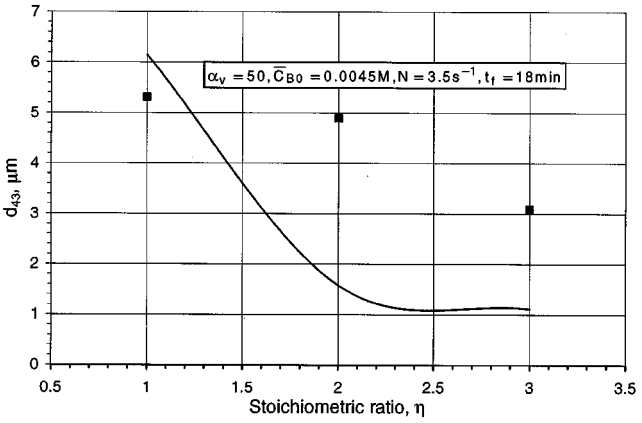

Figure 9. Effect of stoichiometric ratio on mean particle size for feeding near the impeller.

Crystal morphology

The equilibrium shape of a crystal, which corresponds to the lowest energy configuration, results in flat planar surfaces (minimizing the effective surface area). In general, the rosette shaped barium sulfate crystals are orthorhombic in shape with cleavage perfect in one direction, with not as much in the other (see Figure 2a). The crystal morphology is related to the supersaturation profile, which is directly influenced by the mode of feed addition. Figure 12 shows the supersaturation profile for the two modes of feed addition. The supersaturation ratio can be calculated as

$$S = (C_A C_B / K_s)^{1/2} \tag{31}$$

When feeding below the surface of the liquid, high supersaturation ($S > 1{,}000$) results in homogeneous nucleation for a longer time period. This explains the formation of larger crystals in general when feeding near the impeller.

It is expected that the history of supersaturation composition affects crystal morphology in conjunction to the supersaturation profile (Baldyga et al., 1995). That is, the same level of supersaturation can be obtained with different values

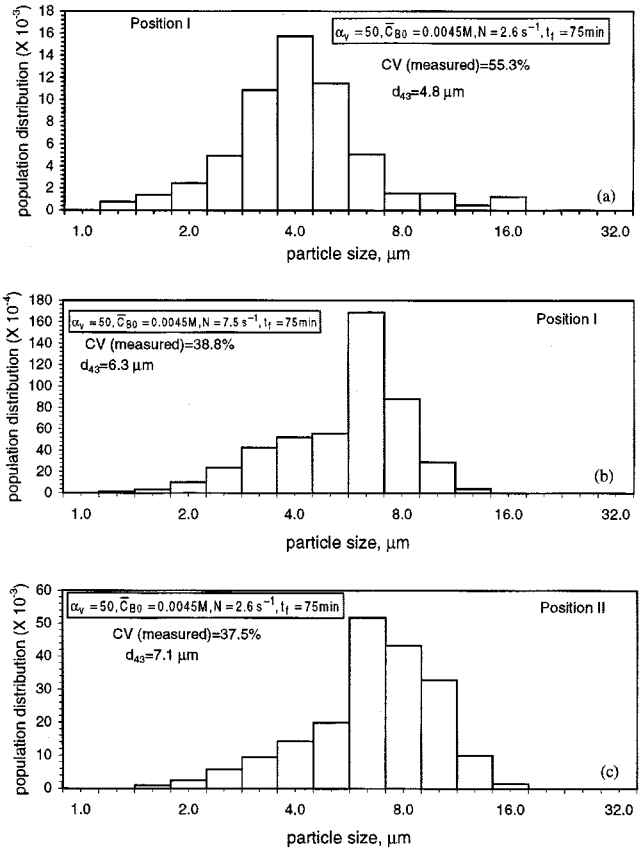

Figure 10. Effect of stirrer speed on C.V. (experimental results).

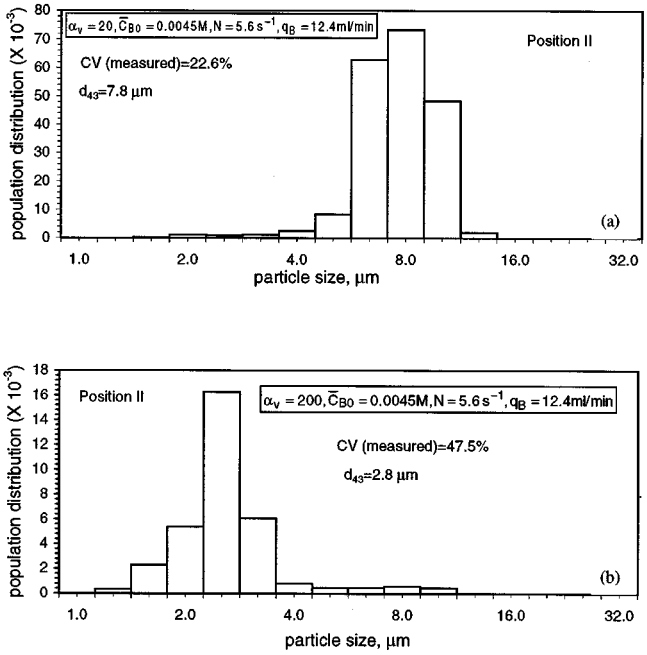

Figure 11. Effect of volume ratio on C.V. (experimental results for feeding near the impeller).

of C_A and C_B (A and B concentrations in the MP-zone), which constitute the supersaturation profile. The supersaturation composition in the MP-zone can be illustrated by using *precipitation diagrams* (Füredi-Mihofer and Walton, 1981), which are plots of pA vs. pB (see Figure 13), where $pA = -\log[A]$ and $pB = -\log[B]$. The position of the region of precipitation on this precipitation diagram determines the crystal morphology. There is no significant difference in the supersaturation composition for the two different feed point locations, in contrast to the precipitation diagrams obtained for the case of a double-feed semi-batch precipitation process (Baldyga et al., 1995). For both feed point locations in the single-feed process, high supersaturation occurs (see Figure 12), whereby the growth process can be controlled by diffusion of the ions in depletion—the diffusional effects can thus control the resulting shape of crystals.

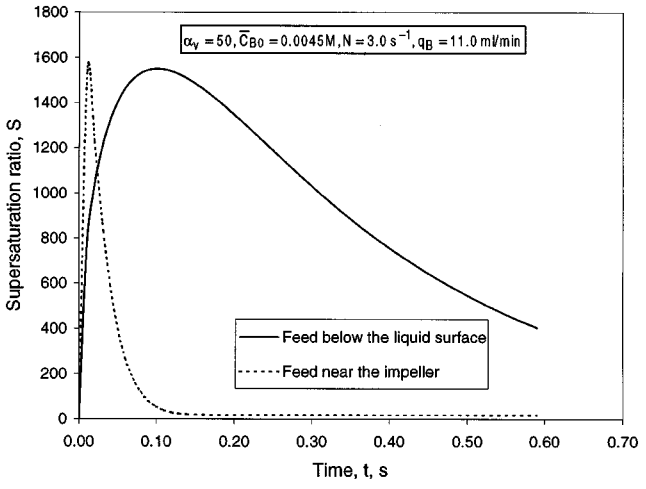

Figure 12. Supersaturation profiles for the two feed addition positions.

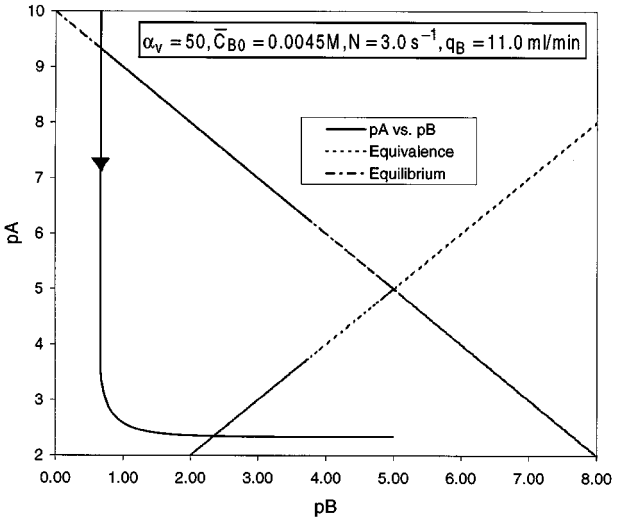

Figure 13. Precipitation diagram illustrating the composition of the MP-zone (initial part of feeding) for feed pipe locations I and II (same profile).

Figure 2b illustrates an SEM photograph of barium sulfate crystals when feeding below the liquid surface and at an initial concentration of barium chloride of 0.0210 mol dm^{-3}. It illustrates the transition of dendritic growth occurring at 0.0100 mol·dm^{-3} (Fitchett and Tarbell, 1990) to the less orderly appearance due to microcrystalline aggregation at still higher concentrations, ~0.0500 mol·dm^{-3} (Fitchett and Tarbell, 1990). The base plane in Figure 2b is slightly irregular and has four branches that appear to be the remnants of a dendritic structure and orthogonal planes. Dendritic crystals are formed when ionic transport in the solution becomes rate governing. This occurs over a supersaturation range in which surface processes do not affect growth, while still below the critical supersaturation for homogeneous nucleation (Füredi-Milhofer and Walton, 1981). At very high concentrations, microcrystalline aggregation occurs probably due to dendritic fragmentation, which is quite typical of barium sulfate crystals. It follows from above that in a single-feed semi-batch precipitation process (contrary to double-feed), crystal morphology is more sensitive to initial reactants' concentration than to the feed pipe location. Moreover, the maximum rate of precipitation (at maximum supersaturation), corresponding to strongly nonequivalent mixtures of Ba^{2+} and SO_4^{2-} ions, is higher in the case of a double-feed process whereby the crystals formed have a larger surface area than for single-feed at both feed addition points.

Conclusion

Application of the E-model to interpret experimental data in a single-feed semi-batch precipitation process at low feed rates was studied. Results of experiments outline the effect of various parameters (feed volume ratio, stirrer speed, feed

addition time, mean initial reactants concentration, and stoichiometric ratio) on the PSD and morphology. It is demonstrated that by modeling the spatial inhomogeneity due to nonideal mixing, the final product properties can be predicted by a simple mechanistic model based, however, on physics of mixing. Application of the model is limited to $1 \ll Sc < 4{,}000$ and low feed rates. The disagreement between the simulation and experimental results was largely due to neglecting nuclei agglomeration and microcrystalline-aggregation (at higher concentrations) in the model. Incorporating more reliable precipitation kinetics for both stoichiometric and nonstoichiometric conditions (Aoun et al., 1996), and using activity instead of the concentration of reactants, should provide a still better agreement of experimental data with model predictions.

Acknowledgment

The first two authors acknowledge financial support from the Natural Sciences and Engineering Research Council of Canada.

Notation

a = specific surface area of the crystals per unit volume of the suspension, dm^2/dm^3
C_1 = bulk entrainment coefficient
C_2 = impeller discharge coefficient
$C_A, [A]$ = concentration of reactant A in the MP-zone, mol/dm^3
$C_B, [B]$ = concentration of reactant B in the MP-zone, mol/dm^3
C_{A0}, C_{B0} = mean initial concentration of A, B, mol/dm^3
$\overline{Cc}$ = mean concentration of precipitating substance, mol/dm^3
$C_i, [i]$ = concentration of reactant i, mol/dm^3
C_{io} = feed concentration of reactant i, mol/dm^3
C_{ij} = concentration of i in j zone, mol/dm^3
$\langle C_i \rangle$ = concentration of reactant i in environment, mol/dm^3
d = impeller diameter, m
d_B = radial distance of feed point, cm
d_m = molecular diameter, dm
D = tank diameter, m
D_i = molecular diffusivity, dm^2/s
D_t = turbulent diffusivity, m^2/s
H = height of liquid in the reactor, dm
k_d = mass-transfer coefficient, dm/s
k_D, k_{DA}, k_{DB} = mass transfer, $(dm/s)\cdot(dm/mol)$
k_N = rate constant for nucleation, $(dm/s)\cdot(dm^6/mol^2)$
k_R = rate constant for surface reaction, $(dm/s)\cdot(dm^6/mol^2)$
L = size of the crystals, dm
m_j = jth moment of a particle size distribution, dm^j/dm^4
M = molar mass of the precipitate, g/mol
MP = mixed-precipitation zone
n^* = number of ions required to form a critical nucleus
q_c = circulation capacity, dm^3/s
q_B = feed rate of reactant B, mL/min., m^3/s
Q_P = pumping capacity of the impeller, dm^3/s
r_x = radial coordinate
R = rate of creation of component i, $mol/(dm^3\cdot s)$
t' = Lagrangian time, age of the blob, s
t = time of semi-batch operation, s
t_c = circulation time, s
t_G = characteristic time constant for crystal growth, s
t_{ms} = characteristic time constant for inertial-convective mixing, s
V = reactor volume, dm^3
V_j = flow rate of the mixed-precipitation zone, dm^3/s
$V_{i,b}$ = volume of the impeller and bulk zones, dm^3
W_b = reactor volume, dm^3
W_b = width of baffles, cm
z = axial coordinate

Greek letters

$\bar{\epsilon}$ = average energy dissipation rate, m^2/s^3
Λ_c = integral scale for concentration fluctuations, m
ν = kinematic viscosity, m^2/s
ρ = density of crystals, g/dm^3
τ_D = characteristic time constant for turbulent diffusion, s
$\phi_{i,b}$ = ratio of local to average mean energy dissipation rate
ϕ_v = sphericity of crystals

Literature Cited

Aoun, M., E. Plasari, R. David, and J. Villermaux, "Are Barium Sulfate Kinetics Sufficiently Known for Testing Precipitation Reactor Models?", *Chem. Eng. Sci.*, **51**, 2449 (1996).

Aslund, B. L., and A. C. Rasmuson, "Semibatch Reaction Crystallization of Benzoic Acid," *AIChE J.*, **38**, 328 (1992).

Baldyga, J., and J. R. Bourne, "A Fluid Mechanical Approach to Turbulent Mixing and Chemical Reaction," *Chem. Eng. Comm.*, **28**, 231 (1984).

Baldyga, J., and J. R. Bourne, "Interactions between Mixing on Various Scales in Stirred Tank Reactors," *Chem. Eng. Sci.*, **47**, 1839 (1992).

Baldyga, J., and W. Orciuch, "Closure Problem for Precipitation," *Trans. Instn. Chem. Engrs.*, Part A, **75**, 160 (1997).

Baldyga, J., and S. Rohani, "Micromixing Described in Terms of Inertial-Convective Disintegration of Large Eddies and Viscous Convective Interactions among Small Eddies I. General Development and Batch Systems," *Chem. Eng. Sci.*, **42**, 2597 (1987).

Baldyga, J., W. Podgórska, and R. Pohorecki, "Mixing Precipitation Model with Application to Double-Feed Semibatch Precipitation," *Chem. Eng. Sci.*, **50**, 1281 (1995).

Bourne, J. R., and S. Yu, "Investigation of Micromixing in Stirred Tank Reactors Using Parallel Reactions," *Ind. Eng. Chem. Res.*, **33**, 41 (1994).

Chen, C., C. Zhang, and G. Chen, "Interaction of Macro and Micromixing on Particle Size Distribution in Reactive Precipitation," *Chem. Eng. Sci.*, **51**, 1957 (1996).

Corrsin, S., "The Isotropic Turbulent Mixer: II. Arbitrary Schmidt Number," *AIChE J.*, **10**, 870 (1964).

David, R., and J. Villermaux, "Interpolation of Micromixing Effects on Fast Consecutive-Competing Reactions in Semi-Batch Stirred Tanks by a Simple Interaction Model," *Chem. Eng. Commun.*, **54**, 333 (1987).

David, R., and B. Marcant, "Prediction of Micromixing Effects in Precipitation: Case of Double Jet Precipitators," *AIChE J.*, **40**, 424 2 (1994).

Dirksen, J. A., and T. A. Ring, "Fundamentals of Crystallization: Kinetic Effects on Particle Size Distributions and Morphology," *Chem. Eng. Sci.*, **46**, 2389 (1991).

Fitchett, D. E., and J. M. Tarbell, "Effect of Mixing on the Precipitation of Barium Sulfate in an MSMPR Reactor," *AIChE J.*, **36**, 511 (1990).

Fort, I., "Flow and Turbulence in Vessels with Axial Impellers," *Mixing. Theory and Practice*, Vol. III, V. W. Uhl and J. B. Gray, eds., Academic Press, Orlando, p. 133 (1986).

Füredi-Milhofer, H., and A. G. Walton, "Principles of Precipitation of Fine Particles," *Dispersion of Powders in Liquids*, Parfitt Applied Science Publishers, NJ (1981).

Garside, J., and N. S. Tavare, "Mixing Reaction and Precipitation Limits of Micromixing in an MSMPR Crystallizer," *Chem. Eng. Sci.*, **40**, 1485 (1985).

Geiser, R. K., "Fluiddynamik und Leistungseintrang in Turbulent Geruehrten Suspensionen," PhD Thesis, Universitaet Muenchen (1991).

Karpinski, P. H., "Importance of the Two Step Particle Growth Model," *Chem. Eng. Sci.*, **40**, 641 (1985).

Kuboi, R., M. Harada, J. M. Winterbottom, A. J. S. Anderson, and A. W. Nienow, "Mixing Effects in Double-Jet and Single-Jet Precipitation," *Proc. of World Congress III of Chemical Engineering*, Tokyo, Japan, Paper 8g, 4 (1986).

Marcant, B., and R. David, "Experimental Evidence for and Prediction of Micromixing Effects in Precipitation," *AIChE J.*, **37**, 1698 (1991).

Nagata, S., and M. Nishikawa, paper read at the Meeting of First Pacific Chem. Eng. Congress (1975) (cited from Nagata, S., *Mixing, Principles and Applications*, Halsted Press (Wiley), New York (1972).
Nielsen, A. E., ''The Kinetics of Crystal Growth in Barium Sulfate Precipitation,'' *Acta Chem. Scand.*, **12**, 951 (1958).
Okamoto, Y., M. Nishikawa, and K. Hashimoto, ''Energy Dissipation Rate Distribution in Mixing Vessels and Its Effect on Liquid-Liquid Dispersion and Solid-Liquid Mass Transfer,'' *Int. Chem. Eng.*, **21**, 88 (1981).
Oldshue, J. Y., ''Fluid Mixing Technology and Practice,'' *Chem. Eng.*, 82 (Jun. 1983).
Pipino, M., A. A. Barresi, and R. O. Fox, ''A PDF Approach to the Description of Homogeneous Nucleation,'' in *Proc. of Quarto Convegno Internazionale Fluidodinamica Multifase Nell'impiantistica Industrialles*, Ancona, Italy (1994).
Pohorecki, R., and J. Baldyga, ''The Use of a New Model of Micromixing for Determination of Crystal Size in Precipitation,'' *Chem. Eng. Sci.*, **38**, 79 (1983).
Podgórska, W., ''Influence of Micromixing on Precipitation,'' PhD Thesis, Warsaw Univ. of Technology, Poland (1993).
Post, T. A., ''Geometrical Influence on Local Mass and Heat Transfer in an Agitated Tank,'' PhD Thesis, Diss. ETH No. 7249, ETH, Zurich, Switzerland (1983).
Randolph, A. D., and M. A. Larson, *Theory of Particulate Processes*, Academic Press, New York (1988).
Templeton, Ch. C., *J. Chem. Eng. Data*, **5**, 514 (1960).
Tosun, G., ''An Experimental Study of the Effect of Mixing on the Particle Size Distribution in $BaSO_4$ Precipitation Reaction,'' *Proc. Europ. Conf. Mixing*, Pavia, Italy, p. 161 (1988).
Uhl, V. W., and J. B. Gray, *Mixing Theory and Practice Vol. I*, Academic Press, New York (1966).
Wei, H., and J. Garside, ''Application of CFD Modelling to Precipitation Systems,'' *Trans. Inst. Chem. Eng.*, **75A**, 219 (1997).
Wu, H., and G. K. Patterson, ''Laser-Doppler Measurements of Turbulent-Flow in Parameters in Stirred Mixer,'' *Chem. Eng. Sci.*, **44**, 2207 (1989).
Zhou, G., and S. M. Kresta, ''Distribution of Energy between Convective and Turbulent Flows for Three Frequently-Used Impellers,'' *Trans. I Chem. E*, **74A**, 379 (1996a).
Zhou, G., and S. M. Kresta, ''Impact of Tank Geometry on the Maximum Turbulence Energy Dissipation Rate for Impellers,'' *AIChE J.*, **42**, 2476 (1996b).

Manuscript received Apr. 13, 1998, and revision received Oct. 20, 1998.